

Solvolysis process of organophosphorus compound *P*-[2-(dimethylamino)ethyl]-*N,N*-dimethylphosphonamidic fluoride with simple and α -nucleophiles: a DFT study

Manoj K. Kesharwani · Md. Abdul Shafeeuulla Khan ·
Tusar Bandyopadhyay · Bishwajit Ganguly

Received: 20 September 2009 / Accepted: 14 November 2009 / Published online: 3 December 2009
© Springer-Verlag 2009

Abstract Density functional theory (DFT) has been used to study the solvolysis process of the organophosphorus compound *P*-[2-(dimethylamino)ethyl]-*N,N*-dimethylphosphonamidic fluoride (GV) with simple nucleophile [hydroxide (HO^-)] and α -nucleophiles [hydroperoxide (HOO^-) and hydroxylamine anion (NH_2O^-)]. The lowest energy conformer of GV used for the solvolysis process was identified with Monte Carlo conformational search (MCOMM) algorithm employing MMFFs force field followed by DFT calculations. The profound effect was found for α -nucleophiles toward the solvolysis of GV compared to normal alkaline hydrolysis. Incorporation of solvent (water) employing SCRFF (PCM) model at B3LYP/6-31+G* showed that solvolysis of GV with hydroperoxide (activation energy = 7.6 kcal/mol) is kinetically more favored compared to hydroxide and hydroxylamine anion (activation energy = 11.0 and 9.2 kcal/mol, respectively). The faster solvolysis of GV with hydroperoxide is achieved due to strong intermolecular hydrogen bonding in the transition state geometry compared to similar α -nucleophile hydroxylamine anion. Assistance of a water molecule

in solvolysis of GV affects the activation barriers; however, the hydroperoxidolysis remains the preferential process. The topological properties of electron density distributions for ($-\text{X}-\text{H}\cdots\text{O}$, $\text{X} = \text{O}, \text{N}$) intermolecular hydrogen bonding bridges have been analyzed in terms of Bader theory of atoms in molecules (AIM). Further, the analysis was extended by natural bond orbital (NBO) methods for the strength of intermolecular hydrogen bonding in the transition state geometries. This study showed that the reactivity of these α -nucleophiles toward the solvolysis of GV is a delicate balance between the nucleophilicity and hydrogen-bond strength. Solvation governs the overall thermodynamics for the destruction of GV, which otherwise is unfavored in the gas phase studies.

Keywords Solvolysis · Ab initio calculations · α -Nucleophiles · Nerve agent · Hydroxylamine anion

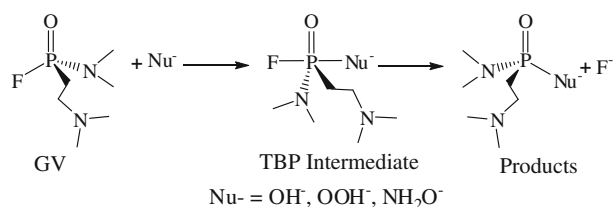
1 Introduction

Detoxification of extremely toxic chemical warfare agents (CWA) such as VX, GB (sarin) and sulfur mustard is an active field of research. Most of the chemical warfare nerve agents are alkylphosphonate and insecticides are generally organophosphate triesters that can irreversibly react with the enzyme acetylcholinesterase (AChE), inhibiting its control over the central nervous system [1–3]. AChE catalyzes the ester hydrolysis process of the neurotransmitter acetylcholine (ACh) to terminate synaptic transmission [4–6]. Inhibition of AChE occurs as a result of the phosphorylation of the active serine residue with organophosphorus compounds [7–9]. AChE inhibition results in acetylcholine accumulation at cholinergic receptor sites, thereby excessively stimulating the cholinergic receptors. This can lead to various

Electronic supplementary material The online version of this article (doi:10.1007/s00214-009-0701-2) contains supplementary material, which is available to authorized users.

M. K. Kesharwani · Md. A. S. Khan · B. Ganguly (✉)
Analytical Science Discipline,
Central Salt and Marine Chemicals Research Institute
(Council of Scientific and Industrial Research),
Bhavnagar 364002, Gujarat, India
e-mail: ganguly@csmcri.org

T. Bandyopadhyay
Theoretical Chemistry Section, Chemistry Group,
Bhabha Atomic Research Centre, Trombay,
Mumbai 400085, India



Scheme 1 Solvolysis process of GV with nucleophiles

clinical disorders. Remediation of such toxic contaminants therefore continues to be a challenge for research groups. In particular, chemical means of achieving efficient destruction of organophosphate esters, especially a facile hydrolysis process, is one of the prime focuses in recent time [10, 11]. Other destruction methods have also been applied using oxidizing agents, photocatalysis, metal-catalyzed decomposition, enzyme degradation and reduction [12–22]. Nerve agents mainly classified as volatile G-series and non-volatile V-series. In addition, another type of nerve agent, whose toxicity falls within G- and V-series is also reported. GV (*P*-[2-(dimethylamino)ethyl]-*N,N*-dimethylphosphonamidic fluoride) is one of the examples of this series [23, 24]. The volatility of GV is in between the V- and G-series nerve agents [23]. One of the chemical means to detoxify GV is solvolysis using nucleophiles [25].

Computational methods offer the ability to explore mechanistic details of these reactions while avoiding exposure to these deadly agents [10, 26–33]. The literature lacks information on solvolysis of GV with typical nucleophiles; however, the reactions with the oxime HI-6 is reported [34]. In the present article, we have computationally explored the solvolysis process of organophosphorus compound GV (Scheme 1) using simple nucleophile viz. hydroxide (HO^-) and α -nucleophiles viz. hydroperoxide (HOO^-) and hydroxylamine anion (NH_2O^-). The calculated results demonstrate that α -nucleophiles are more potent destructing agent for GV compared to that of typical nucleophile. The detailed solvolysis pathways for the destruction of GV with hydroxide, hydroperoxide and hydroxylamine anion (NH_2O^-) are discussed in this study. The potential energy surface for the reactions of GV with these nucleophiles was computed in both gas and aqueous phase. GV is a flexible molecule, hence a detailed conformational search was performed combining Monte Carlo conformational search [35, 36] with MMFFs force field [37–41] and DFT calculations. The details of calculations are given in the computational section.

2 Computational methodology

The following protocol was used to generate conformations of GV. (1) An exhaustive conformational search was

performed with the molecular modeling program MacroModel [42] using MMFFs force field [37–41]. Energy minimizations were performed with the Polak–Ribiere [43] conjugate gradient (PRCG) method, which involves the use of first derivatives with convergence criterion set to 0.05 kJ/Å mol. Conformational search was performed by the Monte Carlo method [35, 36] for the random variation of all of the rotatable bonds combined with the Monte Carlo conformational search (MCM) algorithm [35, 36] using 5000 Monte Carlo steps. (2) Sort all found conformations according to energy. (3) Stored conformations whose relative energy was within 50 kJ/mol of the lowest energy structure. The resulting conformations were clustered based on torsional RMS using XCluster approach [44]. Based on the minimum separation ratio, we have selected clustering level with six clusters. Minimum separation ratio was employed to find the clustering level at which the distance between members of clusters is much smaller than the distance between clusters [45]. Six representative conformers were selected from this clusterization process. The selected conformations from the conformational families were stored for further higher level DFT calculations.

The six selected low energy conformers were optimized with Becke3 Lee–Yang–Parr method [46–48] using 6-31G* basis set [49] in both gas and aqueous phases. The lowest energy conformer was taken to explore the potential energy surface for the reaction of hydroxide, hydroperoxide and hydroxylamine anion with GV. All DFT calculations were performed with Gaussian 03 suite program [50]. All geometries were optimized at B3LYP/6-31G* energy level of theory. To calculate the energies with higher basis set, single point calculations were performed at B3LYP/6-31+G* level using B3LYP/6-31G* optimized geometries. To account for the solvation effect, full geometry optimizations of all stationary points were performed in water using polarizable continuum solvation model (PCM) [51–55] at B3LYP/6-31G* level. For solvent calculation, the program by default builds up the molecular cavity using the united atom (UA0) model [53], i.e., by putting a sphere around each solute heavy atom: hydrogen atoms are enclosed in the sphere of the atom to which they are bonded. The UA0 radii indicate the use of united atom topological model applied on atomic radii of the UFF force field. Further, single point calculations have been performed at B3LYP/6-31+G*/B3LYP/6-31G* level in aqueous phase. The energies calculated at B3LYP/6-31+G* level were corrected with zero-point vibrational energies (ZPVE) obtained at B3LYP/6-31G* level. To examine the reliability of the methods employed in this study, additional calculations were performed for the hydrolysis of two organophosphorus compounds sarin (G-series nerve agent) and methoxy-methyl-phosphoryl fluoride (MMPF) in aqueous

phase. Activation energies for the hydrolysis of these two compounds were calculated using various DFT methods viz. hybrid meta-GGA method (B3LYP, TPSS1KCIS and M05-2X) [56–58] and hybrid DFT method (B3LYP) using 6-31+G* basis set. ZPVE corrected activation energies are given in Table 1. Hybrid meta-GGA functionals B3LYP and TPSS1KCIS considered to be better density functional methods for predictions of thermochemical properties; whereas, M05-2X also known to be a better DFT functional for thermochemistry and non-covalent interactions [56–58]. The calculated activation barriers for the hydrolysis of sarin and **MMPF** with these DFT methods show that B3LYP/6-31+G* activation barriers were found to be in close agreement with the reported experimental results compared to other DFT functionals employed in this study (Table 1) [59]. The better agreement with the experimental results was obtained at B3LYP/6-31+G*//B3LYP/6-31G* level corrected with B3LYP/6-31G* calculated ZPVE values (Table 1).

The stationary points were characterized by frequency calculations in order to verify that the transition structures had one, and only one, imaginary frequency. To verify that each saddle point connects two minima, intrinsic reaction coordinate (IRC) calculations of transition states were performed in both directions, i.e., by following the eigenvectors associated with the unique negative eigen value of the Hessian matrix, using the González and Schlegel [60, 61] integration method. The nature of intermolecular hydrogen bonding in the transition state geometries has been studied by means of the Bader theory of atoms in molecules (AIM) [62–64]. Such analysis was performed, because it is known that the electronic density at the bond critical point (BCP)— ρ_{BCP} and its Laplacian $\nabla^2\rho_{\text{BCP}}$ —may be very useful parameters for the estimation of the relative strength of hydrogen bonding [65]. Additionally,

Table 1 Computed activation energy (kcal/mol) and activation enthalpy (in parentheses) for hydrolysis of organophosphorus compounds **MMPF** and sarin in aqueous phase using different DFT functionals

Method	MMPF ^a	Sarin ^a
B3LYP/6-31+G*	5.3 (4.4)	6.8 (6.0)
BB1 K/6-31+G*	3.8 (3.0)	5.0 (4.3)
TPSS1KCIS/6-31+G*	4.4 (3.5)	5.4 (4.7)
M052X/6-31+G*	1.1 (0.2)	2.6 (1.8)
B3LYP/6-31+G*//B3LYP/6-31G*	7.5 ^a (6.1)	8.6 ^b (7.5)

Arrhenius activation barrier is converted to activation enthalpy for comparison purpose based on the relationship $E_a = \Delta H^\ddagger + RT$, at 298 K

^a Reported experimental activation energy and activation enthalpy for **MMPF** is 10.5 ± 0.7 and 9.9 ± 0.7 kcal/mol, respectively, and for sarin is 9.1 ± 0.3 and 8.5 ± 0.3 kcal/mol, respectively

^b Corrected with B3LYP/6-31G* calculated ZPVE

natural bond orbital (NBO) [66] analysis was also performed.

3 Results and discussion

Six conformations of GV obtained using MMFFs force field are given in Fig. S1 (Supporting information). These conformers are largely different in the relative orientations of substituted amino-groups. Optimization of these six conformers with B3LYP/6-31G* level in both gas phase (Fig. S2, Supporting information) and aqueous phase (Fig. 1) resulted in five different geometries. GV-5 and GV-6 (Fig. S1, Supporting information) yielded the same geometry V shown below (Fig. 1) in both the gas and aqueous phases. The second lowest conformer (GV-2) obtained from Monte Carlo conformational search method was found to be the lowest energy conformer II at DFT level of theory (Fig. 1; Supporting information Figs. S1, S2). The conformer IV is the second lowest energy conformer with inverted pyramidalization of one of the amino nitrogen with respect to the lowest energy conformer (Fig. 1). The conformer II-G (Fig. S2, Supporting information) and II (Fig. 1) has been considered for the solvolysis study with different nucleophiles in gas and aqueous phases, respectively.

It has been anticipated that solvolysis of organophosphorus nerve agents proceeds through the formation of a trigonal-bipyramidal intermediates (TBP) [29]. Generally,

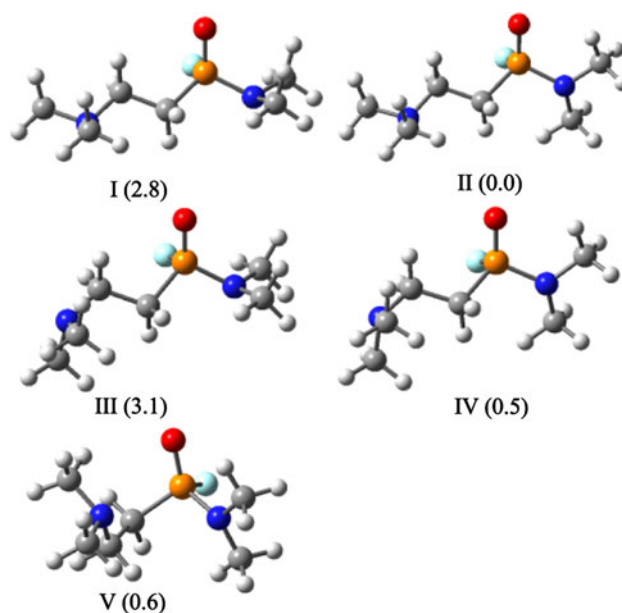


Fig. 1 B3LYP/6-31G* optimized geometry in aqueous phase of various conformer of GV and their relative energies (kcal/mol) compared to conformer II (red oxygen, blue nitrogen, white hydrogen, cyan fluoride and yellow phosphorus)

in trigonal–bipyramidal phosphorus compounds, the most electronegative group thermodynamically prefers the apical position, and also elimination is more facile from an apical position [67]. Thus, the most electronegative group may be expected to be the preferred leaving group in the absence of any other electronic or steric reasons. In the case of GV, fluoride is more electronegative compared to that of other groups, therefore more apicophilic and is more facile leaving group. Reports on GV series of compounds showed that hydrogen fluoride is formed upon hydrolysis [23]. In this study, we have explored the solvolysis process of GV with different nucleophiles assuming the upcoming of nucleophiles opposite to fluorine.

3.1 Hydrolysis

The potential energy profiles for the hydrolysis pathway of GV in both the gas and aqueous phases are given in Fig. 2. The gas phase optimized geometries at B3LYP/6-31G* level are given in Supporting information (Fig. S3). Formation of trigonal bipyramidal intermediate **2a** has been proceeded via the transition state **TS1a** showing negative activation energy of 21.7 kcal/mol in the gas phase at B3LYP/6-31+G**/B3LYP/6-31G* level. A plausible calculated energy barrier can never be negative. It is expected that one other stable structure exists between the reactant and the transition state [68]. Thus, there might be a complex formation between reactants and transition states. The complex (**1a**) between GV and hydroxide ion was found at the potential energy surface with the P–O bond distance of 3.749 Å and 26.1 kcal/mol below the separated reactants (Fig. 2; Supporting information, Fig. S3). Further, complex **1a** leads to a trigonal bipyramidal intermediate **2a** with activation energy of 4.4 kcal/mol (Fig. 2). Intermediate **2a** is 36.8 kcal/mol below separated reactants (Fig. 2). The formation of complex **3a** is energetically favored by 1.1 kcal/mol compared to the intermediate **2a**. This process proceeds via another transition state **TS2a** with an

activation energy of 6.6 kcal/mol (Fig. 2). Finally, complex **3a** leads to the hydrolyzed products *P*-(2-(dimethylamino)ethyl)-*N,N*-dimethylphosphonamidic acid (**P1a**) and fluoride ion, which is 14.7 kcal/mol below separated reactants (Fig. 2). Nevertheless, the products are less stable than the corresponding complex **3a** (Fig. 2). Thus, the last step in the potential energy surface is an endothermic process; however, the overall process ensues rapid hydrolysis of GV with hydroxide ion.

B3LYP/6-31+G**/B3LYP/6-31G* calculated results in the aqueous phase using polarized continuum model (PCM) shows a different pattern from gas phase calculated results (Fig. 2). The separated reactants directly go to the transition state **TS1a-aq** in aqueous phase and the activation energy is found to be 11.0 kcal/mol (Fig. 2). The P–O and P–F bond distances in **TS1a-aq** are 2.885 and 1.639 Å, respectively (Fig. 3). Trigonal bipyramidal intermediate **2a-aq** was found to be 4.7 kcal/mol below separated reactants (Fig. 2). The P–O and P–F bond distances in trigonal bipyramidal intermediate geometry **2a-aq** are 1.774 and 1.773 Å, respectively (Fig. 3). Elimination of fluoride ion proceeds through the transition state **TS2a-aq** with a very small activation energy of 0.1 kcal/mol. On going from the intermediate **2a-aq** to transition state geometry **TS2a-aq** the P–F bond distance (2.894 Å) increased by 0.80 Å shows the expulsion of fluoride ion (Fig. 3). Unlike the gas phase profile, the transition state **TS2a-aq** directly goes to the final products, **P1a-aq** and

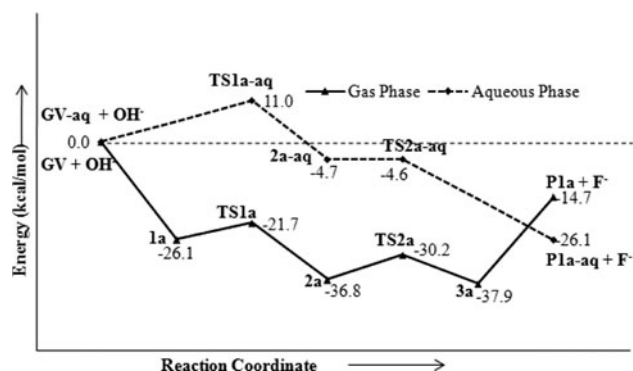


Fig. 2 B3LYP/6-31+G**/B3LYP/6-31G* calculated energy profile diagram for hydrolysis of GV in gas phase and aqueous phase

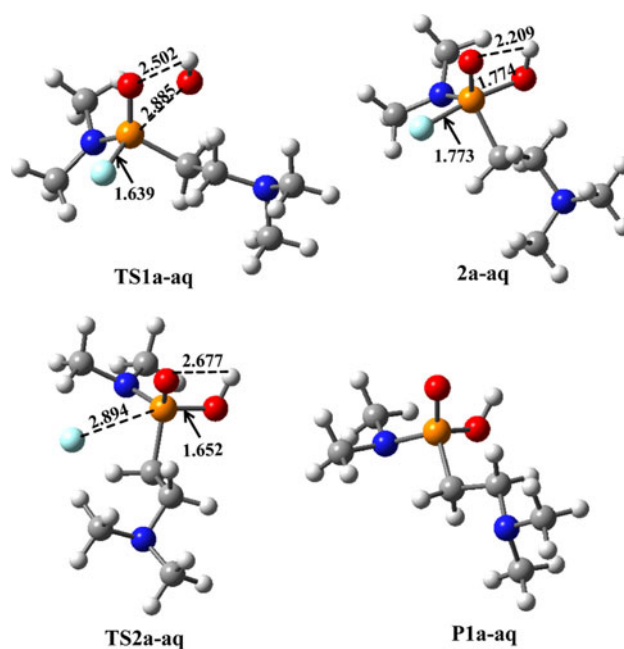


Fig. 3 B3LYP/6-31G* optimized geometries and selected bond distances (Å) for organophosphorus species involved in the hydrolysis of GV in aqueous phase (red oxygen, blue nitrogen, white hydrogen, cyan fluoride and yellow phosphorus)

fluoride ion (Figs. 2, 3). The formation of products is exothermic in the solution phase (Fig. 2). In **P1a-aq**, the hydroxide ion is not participating in the hydrogen bond formation with the dimethylamine group, which however can take place. Optimization of **P1a-aq** with hydrogen bonding between hydroxyl hydrogen and the amino nitrogen leads to a lower energy product (2.0 kcal/mol) compared to the situation where H-bonding is absent. The hydrolysis of GV with hydroxide ion is thermodynamically and kinetically favored in aqueous phase. The higher activation barrier for the formation of transition state **TS1a-aq** than that of transition state **TS2a-aq** reveals that the former transition state would govern the rate of hydrolysis of GV. The solvated stationary points showed the positive barrier for **TS1a-aq** on the reaction coordinate contrary to the gas phase energy profile (Fig. 2). Earlier studies on the nucleophilic substitution at different reaction centers (C, Si and P) have also shown that solvation drastically change the reaction profiles [69–71]. The hydrolysis of GV with M05-2X/6-31+G*/M05-2X/6-31G* level showed similar profile as compared to B3LYP results; however, the predicted activation barrier was found to be 3.3 kcal/mol lower than the later method as observed for sarin and **MMPF** (Figs. S4, S5, Supporting information). The well accounted dispersive forces in M05-2X increases the energy difference between the intermediate **2a-aq** and **TS2a-aq** in the following steps of the hydrolysis process of GV. The calculated hydrolysis process of GV suggests that the activation barrier would be slightly higher than that of similar organophosphorus compound sarin (see computational section). The activation energy predicted for the hydrolysis of sarin in the earlier report also corroborates the results reported herein [28]. GV is bulkier than organophosphorus compound sarin and hence the hydrolysis of GV would be expected to be slightly difficult than that of latter compound as observed in this computational study. Furthermore, the lowering of the activation barrier for sarin could be due to the higher electrophilicity of the reactive phosphorus atom of sarin compared to that of GV due to the presence of more electronegative group $(\text{CH}_3)_2(\text{H})\text{CO}^-$. The calculated Mulliken charge analysis supports that the P atom of sarin is slightly more electro-positive (1.121) than that of the P atom of GV (1.105).

3.2 Hydroperoxidolysis

To examine the effect of α -nucleophiles on solvolysis process of GV, the potential energy surface (PES) was examined with hydroperoxide in the gas and aqueous phase. The calculated PES of hydroperoxide in both phases was found to be similar to that of alkaline hydrolysis of GV. The calculated results are given in Fig. 4 and the stationary points in the gas phase are given in supporting

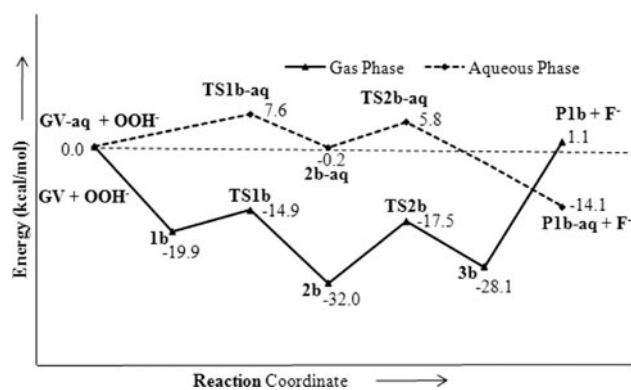


Fig. 4 B3LYP/6-31+G*/B3LYP/6-31G* calculated energy profile diagram for hydroperoxidolysis of GV in the gas and aqueous phases

information (Fig. S6). The formation of products *P*-(2-(dimethylamino)ethyl)-*N,N*-dimethylphosphoramidoperoxoic amide (**P1b**) and fluoride ion in the last step of hydroperoxidolysis is endothermic than the corresponding intermediate **3b** as observed in the hydrolysis of GV (Figs. 2, 4).

The corresponding aqueous phase calculated energy profile and optimized geometries of stationary points of hydroperoxidolysis of GV are given in Figs. 4 and 5, respectively. The activation energy calculated for the first step of hydroperoxidolysis is 7.6 kcal/mol, which is 3.4 kcal/mol lower in energy compared to the corresponding hydrolysis process. The lower activation barrier in **TS1b-aq** compared to **TS1a-aq** is attributed to the presence of strong intermolecular hydrogen bonding interaction between the peroxide hydrogen and one of the oxygen of GV. The hydrogen bonding distance ($-\text{O}\cdots\text{H}$) in **TS1b-aq** is 1.949 Å, which is 0.6 Å shorter than that of **TS1a-aq** (Figs. 3, 5). The P–O and P–F bond distances in **TS1b-aq** are 2.929 and 1.632 Å, respectively, which are comparable to **TS1a-aq**. The next TBP intermediate **2b-aq** is 0.2 kcal/mol below separated reactants (Fig. 4). The P–O and P–F bond distances in intermediate **2b-aq** are 1.835 and 1.731 Å, respectively, and the hydrogen bonding distance between P=O oxygen and $-\text{O}-\text{OH}$ hydrogen shortens further to 1.792 Å (Fig. 5). Elimination of fluoride from GV proceeds in a similar fashion as in hydrolysis mechanism via transition state **TS2b-aq** with activation energy 6.0 kcal/mol. Based on the calculated results it can be concluded that the hydroperoxidolysis would be faster than alkaline hydrolysis of GV (Figs. 2, 4).

3.3 Solvolysis process with hydroxylamine anion

In the series of α -nucleophiles, we have also examined hydroxylamine anion as a nucleophile for solvolysis of GV. It has been reported that the hydroxylamine anion can also be an efficient nucleophile for solvolysis of phosphate

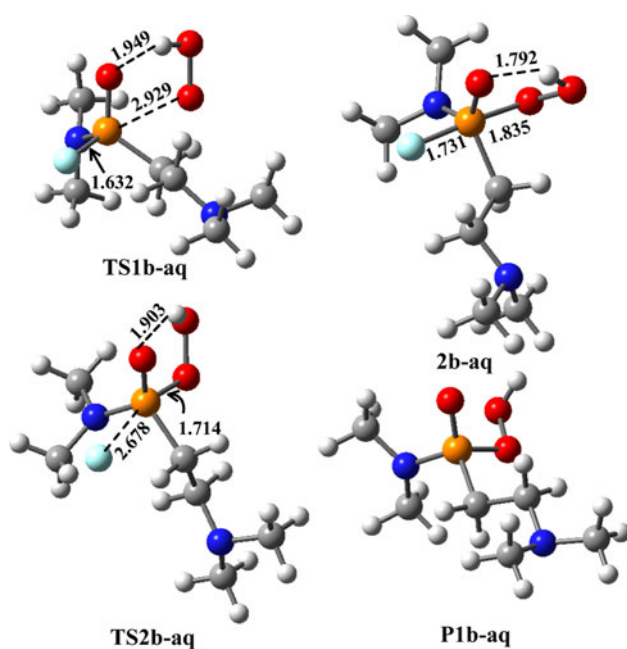


Fig. 5 B3LYP/6-31+G**/B3LYP/6-31G* optimized geometries and selected bond distances (Å) for organophosphorus species involved in the hydroperoxidolysis of GV in aqueous phase (red oxygen, blue nitrogen, white hydrogen, cyan fluoride and yellow phosphorus)

esters [72]. Hydroxylamine was also found to be an oxygen nucleophile, and can exist in three different protonation states depending on the pH [72–74]. Therefore, it is worth to examine the solvolysis process of GV with NH_2O^- . Potential energy surfaces calculated in both the gas and aqueous phases are given in Fig. 6. The optimized geometries of stationary points in the gas phase are given in Fig. S7 (Supporting information) and the stationary points calculated in solvent are shown in Fig. 7. Solvolysis of GV with hydroxylamine anion proceeds in a similar way as observed with hydroxide and hydroperoxide ions. The activation energy for the first transition state (**TS1c**) is 5.3 kcal/mol, which is slightly higher than the

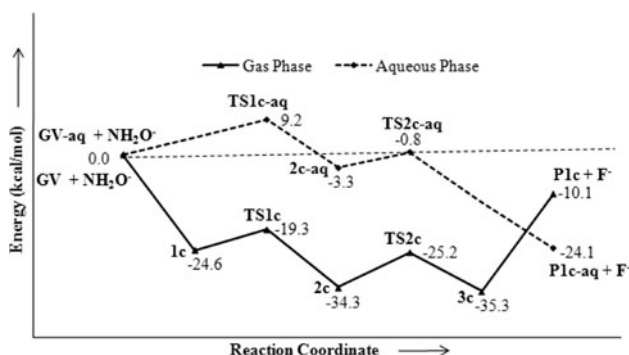


Fig. 6 B3LYP/6-31+G**/B3LYP/6-31G* calculated energy profile diagram for destruction of GV with hydroxylamine anion in gas and aqueous phases

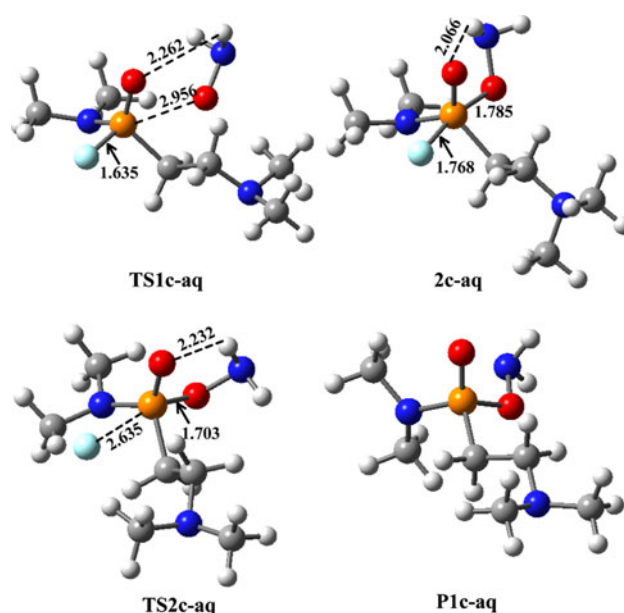


Fig. 7 B3LYP/6-31G* optimized geometries and selected bond distances (Å) for organophosphorus species involved in the solvolysis of GV with hydroxylamine anion in aqueous phase (red oxygen, blue nitrogen, white hydrogen, cyan fluoride and yellow phosphorus)

corresponding activation energies for hydrolysis and hydroperoxidolysis (Fig. 6).

The activation energy calculated in aqueous phase for **TS1c-aq** is 1.8 kcal/mol lower in energy compared to the corresponding transition state with hydroxide (**TS1a-aq**) (Figs. 2, 6); however, 1.6 kcal/mol higher than the corresponding transition state with hydroperoxide (**TS1b-aq**) (Figs. 4, 6). The intermolecular hydrogen bonding distance between GV and hydroxylamine anion in **TS1c-aq** lies within the hydrogen bond distance observed for **TS1a-aq** and **TS1b-aq** (Figs. 3, 5, 7). The relative stabilization of transition states in these cases seems to correlate well with the intermolecular H-bond distances; it is known that the strength of H-bond is dependent on its relative distances [75]. Intermediate **2c-aq** further proceeds to final products **P1c-aq** and fluoride ion via transition state **TS2c-aq**. Comparing the solvolysis rates of GV with the studied α -nucleophiles in aqueous phase, the hydroperoxidolysis should be a facile process than that of hydroxylamine anion. It is to note that the solvent calculations were simulated with implicit continuum model, which does not include explicitly solvent molecules in the process. We therefore examined the influence of a water molecule on the activation barriers of hydroperoxidolysis and solvolysis processes with hydroxylamine anion. The transition state geometries involved in the rate determining steps of hydroperoxidolysis and hydroxylamine anion with GV were modeled with a water molecule bonded to the active center oxygen of (P=O) in aqueous phase (Figs. S8, S9,

Supporting information). The activation energies calculated with a explicit water molecule suggest that the barrier is slightly higher in both hydroperoxidolysis and solvolysis processes with hydroxylamine anion (i.e., 8.2 and 9.6 kcal/mol, respectively); however, the former process is preferred as observed with continuum solvation model calculations. To further examine the influence of more explicit water molecules on the activation energies on both hydroperoxidolysis and solvolysis processes with hydroxylamine anion, additional water molecules were placed around GV with the corresponding α -nucleophiles. Six water molecules were placed near the polar functional groups of GV associated with the α -nucleophiles through hydrogen bonding interactions. Transition state search was performed with explicit water molecules for both hydroperoxidolysis and solvolysis processes with hydroxylamine anion at B3LYP/6-31G* level in continuum solvent (PCM) environment to ensure the surrounding effect of solvent on these transition state geometries. The computed activation energy differences suggest that the hydroperoxidolysis process is ~ 4.0 kcal/mol favored over solvolysis process with hydroxylamine anions (Fig. S10, Supporting information).

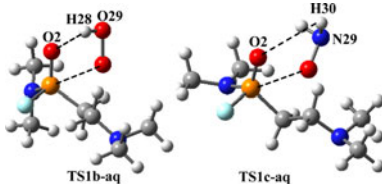
To examine the strength of intermolecular hydrogen bonding, NBO analysis was performed on the transition state geometries for the attack of hydroperoxide (**TS1b-aq**) and hydroxylamine anion (**TS1c-aq**). In Table 2, NBO analysis (occupation number for the assignments and their orbital energies) for the intermolecular hydrogen bonding in transition states and significant donor–acceptor interactions using second order perturbation energies $E^{(2)}$ are reported. The NBO calculated second order perturbative energy for the interaction of lone-pair of donor O2 (n1O2) and σ^* of acceptor unit suggests that such interaction is more favored for **TS1b-aq** than **TS1c-aq** (Table 2) [76]. Further, the Wiberg [77] bond orders calculated for the intermolecular hydrogen bond are higher in the case of

TS1b-aq compared to **TS1c-aq** supporting the stronger hydrogen bonding in the former case (Table 2).

Popelier [78] proposed a set of criteria for the existence of hydrogen bonding within the AIM formalism. Two criteria are connected with electron density, ρ_{BCP} , and its Laplacian, $\nabla^2\rho_{\text{BCP}}$, at (3, -1) critical point (bond critical point, BCP) of two hydrogen-bonded atoms and the others are related to the integrated properties of the H atom. The range of ρ_{BCP} , and its Laplacian, $\nabla^2\rho_{\text{BCP}}$, for normal hydrogen bond is 0.002–0.035 and 0.024–0.139 a.u., respectively [79]. A topological analysis of electronic charge density, ρ_{BCP} , and its Laplacian, $\nabla^2\rho_{\text{BCP}}$, was performed with AIM calculations to gain the knowledge of the intermolecular hydrogen bonds in transition state geometries. The topological parameters evaluated for **TS1b-aq** and **TS1c-aq** are collected in Table 3. It is evident from this table that, in hydrogen bond critical points, ρ_{BCP} and its $\nabla^2\rho_{\text{BCP}}$ are located in the range of 0.002–0.035 and 0.024–0.139 a.u., respectively. These characteristics of electron densities and its Laplacian at BCPs signify the presence of hydrogen bonding interaction. It can also be observed that the electron density and its Laplacian were found to be greater for **TS1b-aq** than that of **TS1c-aq** and support the earlier NBO results (Table 3).

The calculated NBO and AIM topological analyses suggested the stronger intermolecular hydrogen bonding in the case of **TS1b-aq** compared to **TS1c-aq**; however, the relative magnitudes for such interactions were not observed. Howard's [80] proposal to evaluate the hydrogen bond strength using vibrationless model and its components at infinite separations is useful. The magnitudes of intermolecular hydrogen bonding in the transition states were estimated using the transition state geometries of **TS1b-aq** and **TS1c-aq** and their corresponding units separated at infinite separation without perturbing their geometries at B3LYP/6-31+G* level of theory (Fig. S11, Supporting information). The calculated hydrogen bond

Table 2 The NBO analysis data [occupation number (O. N.), their orbital energy E (in a.u.), second order perturbation energy (donor \rightarrow acceptor) (in kcal/mol) and Wiberg bond order] calculated at B3LYP/6-31+G* level of theory for **TS1b-aq** and **TS1c-aq**



Entry	O. N. (n1O2)	E (n1O2)	$n1(\text{O}2) - \sigma^*(\text{X}-\text{Y})^a$	Wiberg B.O. (O2...Y)
TS1b-aq	1.974	-0.726	3.20	0.0336
TS1c-aq	1.976	-0.719	1.15	0.0118

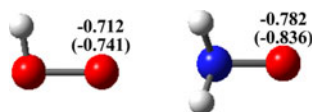
^a X = O29, Y = H28 for **TS1b-aq** and X = N29, Y = H30 for **TS1c-aq**

Table 3 The B3LYP/6-31+G* calculated bond critical point (BCP) data for hydrogen bonds

Entry	Bond (X–Y)	ρ_{BCP}	$\nabla^2\rho_{\text{BCP}}$
TS1b-aq	O2–H28	0.0267	0.0832
TS1c-aq	O2–H30	0.0152	0.0491

strength was found to be 0.5 kcal/mol stronger for **TS1b-aq** than that of **TS1c-aq**.

Comparing the rate determining transition state structures and their stabilities with different nucleophiles, one would like to correlate the reactivity of such nucleophiles with their nucleophilicity as well. The higher reactivity reported for NH_2O^- compared to HOO^- for organophosphorus compound can be correlated well with their nucleophilicity of reactive oxygen atoms [72]. The charge analysis performed for α -nucleophiles, i.e., hydroperoxide (HOO^-) and hydroxylamine anion (NH_2O^-) shows that the nucleophilic oxygen of hydroxylamine anion bears the higher negative charge compared to that of hydroperoxide oxygen atom (Scheme 2). The significance of electronic charges of α -nucleophiles was found to be important to rationalize the hydrolysis of standard nerve agent simulants such as PNPDP and PNP [10]; nevertheless, a direct correlation with quantitative studies was not performed. Importantly, the formation of these nucleophilic anions at a particular pH will be crucial as well to affect the overall solvolysis process of such organophosphorus compounds. The calculated deprotonation energies at the same level of theory suggest that the formation of HOO^- would be easier compared to NH_2O^- (Scheme S1, Supporting information). The computational analyses performed for the solvolysis of GV with hydroperoxide and hydroxylamine anion suggest that the overall process seems to be a delicate balance between nucleophilicity and stabilization of intermediates and transition states through non-bonding interactions like H-bonding. Nevertheless, the solvolysis process carried out under particular conditions can also influence the rate. Therefore, besides the nucleophilicity of nucleophiles, other electronic and structural factors could as well be important to govern the rate of solvolysis of these nerve agents.

**Scheme 2** B3LYP/6-31G* calculated Mulliken and natural charges () for the anionic oxygens in hydroperoxide and hydroxylamine anion (red oxygen, blue nitrogen and white hydrogen)

4 Conclusions

Density functional calculations were carried out on solvolysis of organophosphorus compound GV with hydroxide, hydroperoxide and hydroxylamine anion in both gas and aqueous phase. Mechanistic studies reveal that the reactions are addition–elimination pathway involving trigonal bipyramidal intermediate. Gas phase calculated results showed that the formation of the first transition state is rate determining steps for solvolysis of GV with all nucleophiles studied. The solvolysis of GV is energetically favored in aqueous phase for all the nucleophiles examined. The relative rates of solvolysis of GV with nucleophiles were predicted in the order of $\text{HOO}^- > \text{NH}_2\text{O}^- > \text{HO}^-$. The calculated NBO, AIM results showed that the intermolecular hydrogen bonding is important to reduce the activation barrier for the solvolysis of GV with α -nucleophiles. The reactivity of α -nucleophiles toward the substrate GV seems to be a delicate balance between the nucleophilicity and hydrogen bonding strength. The study rendered some useful information not only for organophosphorus substrates but can also be applicable for other substrates with nucleophiles [81].

Acknowledgments Authors thank DAE-BRNS, Mumbai, India for financial support of this work. One of the authors M.K.K. is thankful to UGC, New Delhi, India for awarding fellowship.

References

- Bunton CA (1997) Chemical warfare. In: Lagowsky JJ (ed) Macmillan encyclopedia of chemistry. Macmillan Reference USA, vol 1. Simon and Schuster Macmillan, New York, pp 343–346
- DeFrank JJ (1991) Organophosphorus cholinesterase inhibitors: detoxification by microbial enzymes. In: Kelly JW, Baldwin TO (eds) Applications of enzyme biotechnology. Plenum Press, New York, pp 165–180
- Heilbronn-Wikstrom E (1965) Sven Kem Tidskr 77:598–631
- Kolb HC, Sharpless KB (2003) Drug Discov Today 8:1128–1137
- Quinn DM (1987) Chem Rev 87:955–979
- Shafferman A, Kronman C, Flashner Y, Leitner M, Grosfeld H, Ordentlich A, Gozes Y, Cohen S, Ariel N, Barak D, Harel M, Silman I, Sussman JL, Velan B (1992) J Biol Chem 267:17640–17648
- Wang J, Roszak S, Gu J, Leszczynski J (2005) J Phys Chem B 109:1006–1014
- Wang J, Gu J, Leszczynski J (2006) J Phys Chem B 110:7567–7573
- Taylor P, Lappi S (1975) Biochemistry 14:1989–1997
- Kumar VP, Ganguly B, Bhattacharya S (2004) J Org Chem 69:8634–8642
- Gershonov E, Columbus I, Zafrani Y (2009) J Org Chem 74:329–338
- Yang YC, Szafraniec LL, Beaudry WT, Rohrbaugh DK (1990) J Am Chem Soc 112:6621–6627
- Simanenko YS, Savelova VA, Prokop'eva TM, Mikhailov VA, Turovskaya MK, Karpichev EA, Popov AF, Gillitt ND, Bunton CA (2004) J Org Chem 69:9238–9240

14. Vorontsov AV, Davydov L, Reddy EP, Lion C, Savinov EN, Smirniotis PG (2002) *New J Chem* 26:732–744
15. Vorontsov AV, Chen YC, Smirniotis PG (2004) *J Hazard Mat* B113:89–95
16. Michalkova A, Gorb L, Ilichenko GM, Zhikol OA, Shishkin OV, Leszczynski J (2004) *J Phys Chem B* 108:1918–1930
17. Keizer TS, Pue De LJ, Parkin S, Atwood DA (2002) *J Am Chem Soc* 124:1864–1865
18. Hill CM, Li WS, Thoden JB, Holden HM, Raushel FM (2003) *J Am Chem Soc* 125:8990–8991
19. Amitai G, Adani R, Hershkovitz M, Bel P, Rabinovitz I, Meshulam H (2003) *J Appl Toxicol* 23:225–233
20. Hoskins FCG, Walker JE, Dettbarn WD, Wild JR (1995) *Biochem Pharmacol* 49:711–715
21. Kiddie JJ, Mezyk SP (2004) *J Phys Chem B* 108:9568–9570
22. Aguila A, O'Shea KE, Tobien T, Asmus KD (2001) *J Phys Chem A* 105:7834–7839
23. Hoenig SL (2007) *Compendium of chemical warfare agents*. Springer, New York, p 100
24. Royo S, Martínez-Mañez R, Sancenón F, Costero AM, Parra M, Gil S (2007) *Chem Commun* 4839–4847
25. Cassagne T, Cristau HJ, Delmas G, Desgranges M, Lion C, Magnaud G, Torreilles É, Virieux D (2001) *Heteroat Chem* 12:485–490
26. Bermudez VM (2007) *J Phys Chem C* 111:9314–9323
27. Bandyopadhyay I, Kim MJ, Lee YS, Churchill DG (2006) *J Phys Chem A* 110:3655–3661
28. Šečková J, Menke JL, Emmett RJ, Patterson EV, Cramer CJ (2005) *J Org Chem* 70:8649–8660
29. Zheng F, Zhan CG, Ornstein RL (2001) *J Chem Soc Perkin Trans* 2:2355–2363
30. Patterson EV, Cramer CJ (1998) *J Phys Org Chem* 11:232–240
31. Daniel KA, Kopff LA, Patterson EV (2008) *J Phys Org Chem* 21:321–328
32. Menke JL, Patterson EV (2007) *J Mol Struct: THEOCHEM* 811:281–291
33. Khan MAS, Kesharwani MK, Bandyopadhyay T, Ganguly B (2009) *J Mol Graphics Modell* 28:177–182
34. Kassa J, Bajgar J (1996) *Acta Med* 39:27–30
35. Chang G, Guida WC, Still WC (1989) *J Am Chem Soc* 111:4379–4386
36. Saunders M, Houk KN, Wu YD, Still WC, Lipton M, Chang G, Guida WC (1990) *J Am Chem Soc* 112:1419–1427
37. Halgren TA (1996) *J Comput Chem* 17:616–641
38. Halgren TA (1996) *J Comput Chem* 17:553–586
39. Halgren TA (1996) *J Comput Chem* 17:520–552
40. Halgren TA (1996) *J Comput Chem* 17:490–519
41. Halgren TA, Nachbar RB (1996) *J Comput Chem* 17:587–615
42. Mohamdi F, Richards NGJ, Guida WC, Liskamp R, Lipton M, Caufield C, Chang G, Hendrickson T, Still WC (1990) *J Comput Chem* 11:440–467
43. Polak E, Ribiere G (1969) *Rev Fr Inf Rech Oper* 16-R1:35–43
44. Shenkin PS, McDonald DQ (1994) *J Comput Chem* 15:899–916
45. Hillson SD, Smith E, Zeldin M, Parish CA (2005) *J Phys Chem A* 109:8371–8378
46. Becke AD (1993) *J Chem Phys* 98:5648–5652
47. Lee C, Yang W, Parr RG (1988) *Phys Rev B* 37:785–789
48. Beck JM, Hadad CM (2008) *Chemico biological interactions* 175:200–203
49. Hehre WJ, Radom L, Schleyer PvR, Pople JA (1988) *Ab initio molecular orbital theory*. Wiley, New York
50. Frisch MJ, Trucks GW, Schlegel HB, Scuseria GE, Robb MA, Cheeseman JR, Montgomery JA Jr, Vreven T, Kudin KN, Burant JC, Millam JM, Iyengar SS, Tomasi J, Barone V, Mennucci B, Cossi M, Scalmani G, Rega N, Petersson GA, Nakatsuji H, Hada M, Ehara M, Toyota K, Fukuda R, Hasegawa J, Ishida M, Nakajima T, Honda Y, Kitao O, Nakai H, Klene M, Li X, Knox JE, Hratchian HP, Cross JB, Adamo C, Jaramillo J, Gomperts R, Stratmann RE, Yazyev O, Austin AJ, Cammi R, Pomelli C, Ochterski JW, Ayala PY, Morokuma K, Voth GA, Salvador P, Dannenberg JJ, Zakrzewski VG, Dapprich S, Daniels AD, Strain MC, Farkas O, Malick DK, Rabuck AD, Raghavachari K, Foresman JB, Ortiz JV, Cui Q, Baboul AG, Clifford S, Cioslowski J, Stefanov BB, Liu G, Liashenko A, Piskorz P, Komaromi I, Martin RL, Fox DJ, Keith T, Al-Laham MA, Peng CY, Nanayakkara A, Challacombe M, Gill PMW, Johnson B, Chen W, Wong MW, Gonzalez C, Pople JA (2004) *Gaussian 03, Revision E.01*. Gaussian, Inc., Wallingford, CT
51. Tomasi J, Persico M (1994) *Chem Rev* 94:2027–2094
52. Cossi M, Barone V, Cammi R, Tomasi J (1996) *Chem Phys Lett* 255:327–335
53. Barone V, Cossi M, Tomasi J (1997) *J Chem Phys* 107:3210–3221
54. Barone V, Cossi M, Tomasi J (1998) *J Comput Chem* 19:404–417
55. Cossi M, Barone V (1998) *J Chem Phys* 109:6246–6254
56. Zhao Y, Lynch BJ, Truhlar DG (2004) *J Phys Chem A* 108:2715–2719
57. Zhao Y, Lynch BJ, Truhlar DG (2005) *Phys Chem Chem Phys* 7:43–52
58. Zhao Y, Schultz NE, Truhlar DG (2006) *J Chem Theory Comput* 2:364–382
59. Larsson L (1957) *Acta Chem Scand* 11:1131–1142
60. González C, Schlegel HB (1990) *J Phys Chem* 94:5523–5527
61. González C, Schlegel HB (1991) *J Chem Phys* 95:5853–5860
62. Bader RFW (1990) *Atoms in molecule: a quantum theory*. Oxford University Press, New York
63. Cioslowski J, Nanayakkara A, Challacombe M (1993) *Chem Phys Lett* 203:137–142
64. Cioslowski J (1994) *Chem Phys Lett* 219:151–154
65. Espinosa E, Souhassou M, Lachekar H, Lecomte C (1999) *Acta Crystallogr B* 55:563–572
66. Glendening DE, Reed AE, Carpenter JE, Weinhold F (1992) *NBO Version 3.1*
67. Thatcher GRJ, Kluger R (1989) *Adv Phys Org Chem* 25:99
68. Zhan C-G, Landry DW, Ornstein RL (2000) *J Am Chem Soc* 122:1522–1530
69. van Bochove MA, Bickelhaupt FM (2008) *Eur J Org Chem* 649–654
70. van Bochove MA, Swart M, Bickelhaupt FM (2007) *Chem Phys Chem* 8:2452–2463
71. van Bochove MA, Swart M, Bickelhaupt FM (2006) *J Am Chem Soc* 128:10738–10744
72. Kirby AJ, Manfredi AM, Souza BS, Medeiros M, Priebe JP, Brandão TAS, Nome F (2009) *ARKIVOC*. (iii):28–38
73. Kirby AJ, Souza BS, Medeiros M, Priebe JP, Manfredi AM, Nome F (2008) *Chem Commun* 4428–4429
74. Kirby AJ, Davies JE, Brandão TAS, da Silva PF, Rocha WR, Nome F (2006) *J Am Chem Soc* 128:12374–12375
75. Anslyn EV, Dougherty DA (2006) *Modern physical organic chemistry*. University Science Books, Sausalito, p 168
76. Raissi H, Jalbout AF, Farsi H, Abbasi B, De Leon A, Moghiminia S (2009) *Int J Quantum Chem* 109:1609–1616
77. Wiberg KB (1968) *Tetrahedron* 24:1083–1096
78. Popelier PLA, Bader RFW (1992) *Chem Phys Lett* 189:542–548
79. Nowroozi A, Jalbout AF, Roohi H, Khalilinia E, Sadeghi M, De Leon A, Raissi H (2009) *Int J Quantum Chem* 109:1505–1514
80. Howard ST (2000) *J Am Chem Soc* 122:8238–8244
81. Simanenkov YS, Popov AF, Prokop'eva TM, Savelova VA, Belousova IA (1994) *Theor Exp Chem* 30:61–64